physica **pss** status solidi **b**

www.pss-b.com

basic solid state physics

Synthesis and characterization of TiO₂/C nanomaterials: Applications in water treatment

Drissa Bamba[1,2,3]**, Mariame Coulibaly**[1,4]**, Carmen I. Fort***[*,2]**, Cosmin L. Coteţ**[2]**, Zsolt Pap**[2,5]**, Krisztina Vajda**[5]**,
Elogne G. Zoro**[1]**, N. Alfred Yao**[4]**, Virginia Danciu****[**,2]**, and Didier Robert*****[***,1,3]

[1] Laboratoire de Chimie des Eaux (LCE), Ecole Normale Supérieure d'Abidjan, 08 BP 10 Abidjan 08, Côte d'Ivoire
[2] Laboratory for Electrochemical Research (LER), Babeş-Bolyai University, 400028 Cluj-Napoca, Romania
[3] Institut de Chimie et Procédés Pour l'Energie, l'Environnement et la Santé (ICPEES), CNRS University of Strasbourg, Saint-Avold Antenna, Université de Lorraine rue Victor Demange, 57500 Saint-Avold, France
[4] Laboratoire des Sciences Physiques Fondamentales et Appliquées, Ecole Normale Supérieure d'Abidjan, 08 BP 10, Abidjan 08, Côte d'Ivoire
[5] Research Group of Environmental Chemistry, Institute of Chemistry, University of Szeged, Tisza Lajos krt. 103, 6720 Szeged, Hungary

* Corresponding author: e-mail iladiu@chem.ubbcluj.ro, Phone: +40264593833, Fax: +40264590818
** e-mail vdanciu@chem.ubbcluj.ro, Phone: +40264593833, Fax: +40264590818
***e-mail didier.robert@univ-lorraine.fr, Phone: +3368850000, Fax: +3368850000

The TiO₂ deposition on high surface possessing supports can increase the photocatalytic efficiency of a semiconductor, as already shown in the literature because, the high adsorption capacity of the support can help to enrich the organic substrate around the catalyst promoting the charge-transfer process between the pollutants and the photocatalysts. Consequently, in this study, we investigated the synthesis of composite photocatalytic materials based on TiO₂ and different types of carbon. Titanium tetrachloride (TiCl₄) was used as the precursor, while graphite, activated carbon and carbon aerogels were chosen as carbon supports. An optimization of the synthesis method was proposed by varying the molar ratio titanium/carbon (Ti/C). The obtained materials were characterized by XRD, TEM, and UV–Vis DRS. The specific surface area, pore volume, and pore-size distribution were evaluated by nitrogen adsorption/desorption. The photocatalytic activity was investigated by the photodegradation of diuron.

1 Introduction Around the world, clean drinking water is the most intriguing problem and it urgently needs to be solved. To provide food for as many people as possible it is necessary to use pesticides (herbicides, fungicides, insecticides, etc.), to improve the yield of the produced vegetables and fruits. Consequently, lots of chemical contaminants are leaching into the environment and accumulating in the ground/groundwater/surface water. This is followed by a second accumulation in the plants and animals, and at the end of this process, humans are also affected. The pesticides are a huge section of the water pollutants, which are mostly nonbiodegradable, and can initialize harmful processes in many organisms, such as cancer by pesticides (e.g., methyl parathion) [1]. Hence, it is mandatory that we should eliminate and/or try to convert most of the harmful organic molecules into carbon dioxide and water.

Nowadays, there are several useful methods to eliminate organic contaminants from water, and one of them is heterogeneous photocatalysis, which is a very attractive technology exploiting the specific ability of semiconductors. Their crucial process is: when a photon (with sufficient energy, e.g., UV light) is absorbed, an electron (e⁻) jumps from the valence band into the conduction band [2] and leaves behind a positively charged hole (h⁺). In heterogeneous photocatalysis many semiconductors have already been applied [3], but titanium dioxide (TiO₂) is the most suitable one due to its beneficial properties: efficient, low

Wiley Online Library

cost, nontoxic, and stable [4]. Moreover, TiO$_2$ is suitable for lots of other applications, such as renewable energy sources [5], and so is well presented in green technologies [6]. The photocatalytic activity of TiO$_2$ is dependent on the surface structure, on the crystal size, crystal phase, crystal shape, and of course the dominance of the reactive crystal facets [7]. From the three crystal phases of the TiO$_2$ the anatase phase shows a better photocatalytic activity than rutile, because rutile has higher recombination rate of the e$^-$/h$^+$ pairs [8]. However, anatase has a relatively large bandgap (≈ 3.2 eV) [9] and only UV (λ: 200–400 nm) in the solar spectrum (about 3–5%) can be utilized to initiate the generation of the charge carriers. Normally, under UV illumination the electrons and holes in the TiO$_2$ have a very short lifetime due to the close proximity of the charge carriers [10, 11]. Therefore, a possible solution of this problem is to increase their (e$^-$, h$^+$) lifetime with their separation: electrons can react with an electron acceptor: e.g., trapped by O$_2$ to form superoxide radical ions ($\bullet$O$_2{}^-$) [12], which in further transformations can lead to formation of $\bullet$OH radicals [13] or the electron can interact with other semiconductors/conductor materials such as single, or multi-walled carbon nanotubes (SW/MWCNTs) [14]. "On the other side" of the redox process: extremely active radicals ($\bullet$OH) can be generated at the semiconductor surface, due to the holes' (h$^+$) reaction: h$^+$ + OH$^-$ $\rightarrow$ $\bullet$OH. A solution to enhance the photocatalytic activity of titania is the coupling of TiO$_2$ with a smaller bandgap semiconductor with a higher conduction band (CB) than TiO$_2$ [15]. Additionally, visible-light sensitivity can be achieved by doping with carbon [16] nitrogen [17] and of course with the deposition of noble metals (Pt, Au) [18].

Various methods have been developed to obtain TiO$_2$ nanoparticles. These efforts were targeted to control different critical parameters, such as the size, shape, and crystal phase composition of the SC (semiconductor). Among the mentioned methods were the sol–gel [19, 20] and the hydrothermal treatments [21]. However, these synthetic methods are based mainly on the reactions containing organic compounds and the removal of the surface anchored organic groups [22, 23] is a challenging process. The synthesis of TiO$_2$ by controlled hydrolysis of TiCl$_4$ offers a promising way to generate TiO$_2$ nanoparticles without uncontrolled carbon deposits. This synthesis generates the TiO$_2$ nanoparticles mainly with anatase phase [24]. It was also shown that different nanocrystallite sizes can be obtained by controlling the temperature of the water and the concentration of TiCl$_4$ [25].

Based on the information provided until this point it is clear that a carbon-free TiO$_2$ precursor should be applied in order to obtain the desired nanoparticles. It is also clear that the charge separation should be promoted. For this purpose the composite materials are the perfect solution as it was shown by many other publications in this field.

The deposition of TiO$_2$ on different materials were performed [26–29], obtaining composites, such as TiO$_2$/SiO$_2$, TiO$_2$/zeolite, and TiO$_2$/carbon. The deposition of TiO$_2$ on activated carbon (AC) according to Gao et al. [30], may increase the efficiency of the photocatalytic material because it can help to enrich the organic substrate around the catalyst and promotes the charge-transfer process between the pollutant and the photocatalyst. This synergistic effect was observed in the case of the degradation of several types of organic pollutants [31–33]. According to Cordero et al. [34], the surface chemistry and activated carbon texture exhibit a significant influence on the aggregation of TiO$_2$ particles, and thus on the photocatalytic degradation of 4-chlorophenol. Gao et al. [30] also studied the synergy between TiO$_2$ and two types of AC and found that the optimal TiO$_2$ to AC mass ratio was 80–20 for the highest photocatalytic activity (degrading Acid Red 88).

Diuron [3-(3,4-dichlorophenyl)-1,1-dimethylurea] is a herbicide from the urea group and the subclass of phenylurea, moreover one of the most commonly used pesticides in Ivory Coast for the intensive agriculture of banana, coffee, cotton, or rice. For example, in the case of banana, the diuron amount used is 4.5–5 kg per hectare and per treatment [35]. Unfortunately, it is one of the highly biorecalcitrant organic contaminants in the hydrosphere, due to industrial and intensive agricultural production [36]. This compound is soluble in water (36.4 mg L^{-1} at 25 °C) and is highly persistent, with a half-life in soil of over 300 days. Another huge problem is the strong toxicity of its main byproducts (3, 4-dichloroaniline and 1-(3, 4-dichlorophenyl) urea [37]. Furthermore, this compound has been selected because it is considered as a priority hazardous substance by the European Commission [38]. According to the French Environmental Institute, in France, diuron is detected in 28% of the samples from rivers in the basin system.

In this study, we present the synthesis of TiO$_2$ by controlled hydrolysis of TiCl$_4$. This process has been applied for the deposition of TiO$_2$ on different carbon materials such as activated carbon, graphite (GR), and carbon aerogel (CA). Since each of the mentioned carbons has different surface properties and various surface textures, they can potentially lead to distinct photocatalytic performance in their composite materials. That is why the main objectives were

(i) to establish the influence of surface chemistry and texture of different carbons on the characteristics and photocatalytic performances of the titania composites, and

(ii) to investigate the synergy between the TiO$_2$ and the different support materials on the photodegradation of diuron.

2 Materials and methods

2.1 Materials
Analytical grade reagents were used as supplied, without further purification. A commercial P25 powder, manufactured by Evonik Company (called now Evonik Aeroxide P25) was used.

Diuron (99.5% purity, N-(3,4-dichlorophenyl)-N, N-dimethyl urea) was purchased from Aldrich Company.

Phys. Status Solidi B 252, No. 11 (2015)

2505

Original

Paper

Graphite powder was acquired from Sigma–Aldrich (particle dimensions were less than $20\,\mu m$).

The used activated carbons are derived from previous studies, where two activation modes (physical and chemical) were presented. These preparation methods are detailed in our previous work [39]. However, in this study, the active carbon was obtained by chemical activation with KOH as the activating agent (carbon/KOH = 10/7.5). This carbon has a relatively low specific surface area ($459.10\,m^2\,g^{-1}$) and low density of surface-anchored organic functional groups. Additionally, it does not have sufficient affinity towards the pollutant, which prevents its complete adsorption.

2.2 Preparation of composites For carbon aerogel preparation, resorcinol (R, 98% purity, Aldrich), formaldehyde (F, 37% solution, Aldrich), Na_2CO_3 (C, 99.9% purity, Merck), and bidistilled water (W) was used [40]. Resorcinol-R was dissolved in bidistilled water-W ($R/W = 0.2\,g\,mL^{-1}$). The formaldehyde solution was added to resorcinol solution ($R/F = 0.5$ molar ratio) under vigorous stirring. A catalytic solution $-C$, $0.1\,M$ of Na_2CO_3 was added dropwise to the previous mixture ($R/C = 500$ molar ratio). The resulted solution was placed into tightly closed glass molds and cured 1 day at room temperature and 4 days at $70\,°C$. After 15 days of aging at room temperature, in a closed glass mold the obtained resorcinol-formaldehyde wet gel was washed with acetone (at least 3 days and $3\times$ with fresh solvent). This wet gel was dried with CO_2 in supercritical condition (more than $74\,atm$ and $32\,°C$) when the aerogel was obtained. Then, the organic sample was pyrolyzed in an Ar atmosphere for $2\,h$ at $750\,°C$, when carbon aerogel was obtained.

Titanium dioxide/carbon nanocomposites were synthesized by the controlled hydrolysis of $TiCl_4$ (Sigma–Aldrich). At a desired stoichiometric amount of carbon, previously washed with deionized water, was added $17.5\,mL$ of concentrated hydrochloric acid (Reagent Grade, 37%). Then, we added $3.5\,mL$ of glacial acetic acid. Finally, $5\,mL$ of $TiCl_4$ was added dropwise in this mixture under vigorous stirring. To avoid the overheating of the reaction vessel, it was cooled on an ice bath maintaining a temperature between $0–5\,°C$. This mixture was added dropwise under intense stirring into $500\,mL$ of deionized water. The final pH was below 1.0 and it was adjusted with an aqueous solution of ammonia (25%) until the pH value of 8 was obtained. The mixture was left for 2 days at room temperature to complete the hydrolysis. The precipitate was dried at $80\,°C$ for $24\,h$ and was calcined in a furnace in still air at $400\,°C$ for $2\,h$. The heating rate was $5\,°C\,min^{-1}$.

The bare (carbon-free) titanium dioxide was also synthesized using the same conditions listed above.

2.3 Elemental analysis and UV–visible spectroscopy Elemental analysis of the obtained materials was performed using a "Euro EA Elemental Analyzer 3000 series". The calibration of the instrument was performed with L-cystine. It focused on the nonmetallic chemical elements such as carbon.

As for the optical properties of the materials, a "JASCO V-650 spectrophotometer" diode array computer controlled (Spectra Manager Software) spectrophotometer with an integration sphere (ILV-724) was used for measuring the diffuse reflectance spectra of the samples between 200 and 800 nm.

2.4 X-ray diffraction (XRD) and TEM X-ray diffraction (XRD) measurements were performed using a BRUKER D8 Advance X-ray diffractometer, working at $45\,kV$ and $45\,mA$. The X-ray diffraction patterns were collected in a step-scanning mode with steps of $\Delta\theta = 0.01°$ using CuK_α radiation ($\lambda = 1.54056\,\text{Å}$) in the 2θ range $15–80°$. The anatase–brookite–rutile phase ratio was evaluated using the method developed in Ref. [41], and the crystallite average size was calculated using the Scherrer equation.

TEM micrographs were recorded on a JEOL JEM 1010 TEM operating at an accelerating voltage of $100\,kV$ and equipped with a MegaView III CCD camera.

2.5 Specific surface area, total pore volume, and pore-size distribution For the determination of the specific surface area, total pore volume and the size, and distribution of the pores, N_2 adsorption/desorption measurements were applied, using a "Micromeritics Tristar 3000." analyzer.

2.6 Photocatalytic activity of nanoparticles synthesized All reactions were performed in a Pyrex cylindrical photoreactor ($1\,L$ capacity, $7\,cm$ deep, and $13.5\,cm$ in diameter). The photocatalytic processes were conducted in the solar box ATLAS SUNTEST CPS+ simulating natural radiation (light source vapor Xenon lamp) [42]. To evaluate the photocatalytic activities of our materials, $500\,mL$ of diuron aqueous solution ([diuron] $= 20\,mg\,L^{-1}$ or $85.8\,\mu mol\,L^{-1}$) with an appropriate weight of TiO_2 ($C_{TiO2} = 1\,g\,L^{-1}$ or $C_{TiO2/C} = 1\,g\,L^{-1}$) were homogenized using magnetic stirring in diuron aqueous solution, until an equilibrium state was achieved in the dark. All experiments were performed at $35\,°C$. The mixtures of contaminants and catalysts were continuously magnetically stirred during photocatalytic tests.

Before analysis, the photocatalyst was separated through the $0.45\,\mu m$ "Millipore MF" membrane filter. Diuron was not adsorbed onto the surface of the membrane filter (verified spectrophotometrically before/after with a solution of diuron $20\,mg\,L^{-1}$, without the photocatalyst).

The concentration of diuron was determined with high-performance liquid chromatography (HPLC waters 600 pump, C-18 apolar column and acetonitrile (70%) water (30%) mixture as mobile phase) or with a LIBRA S12 UV–Vis spectrophotometer ($\lambda_{detection} = 248\,nm$).

The blank experiment, under illumination and without photocatalyst, showed that the photolysis of diuron is negligible under these conditions.

Table 1 The results of the elemental analysis.

sample name	theoretical molar ratio Ti/C	experimental molar ratio Ti/C
TiO$_2$/GR	(1/1)	1.33
TiO$_2$/GR	(1/2)	0.52
TiO$_2$/GR	(2/1)	2.16
TiO$_2$/AC	(1/1)	1.41
TiO$_2$/AC	(1/2)	0.62
TiO$_2$/AC	(2/1)	2.48
TiO$_2$/CA	(1/1)	1.25
TiO$_2$/CA	(1/2)	0.49
TiO$_2$/CA	(2/1)	2.25
bare TiO$_2$	(1/0)	–
graphite	(0/1)	–

Figure 2 Diffuse reflectance spectra of the composite photocatalysts TiO$_2$/activated carbon.

3 Results and discussion
3.1 Nanopowder characterization
3.1.1 Elemental analysis and diffuse reflectance spectroscopy
It is important to know the final carbon content of the materials, to verify if the added carbon content was also preserved after the calcination. The results are shown in Table 1.

Figures 1–3 show the evolution of absorbance towards the incident wavelength of pure TiO$_2$ and TiO$_2$/carbon prepared by sol–gel. At first sight, it is clear that the materials absorb the light in the UV region and can be excited in the visible region, with the exception of the sample containing TiO$_2$ only.

3.1.2 Nitrogen adsorption–desorption isotherms and porous structure
In order to investigate the porous properties of the as-prepared samples, nitrogen adsorption–desorption isotherms were measured. It can be seen from Fig. 4 that the isotherms of all samples revealed a typical type-IV sorption behavior with the hysteresis loop, representing the predominant mesoporous structure characteristic according to the classification of IUPAC [43–45].

The pore-size distributions of samples are illustrated in Fig. 5. TiO$_2$ composites present a uniform pore-diameter distribution with maximum at 7.5 nm. According to Shi et al. [46], these pores could be formed by the accumulation of nanoparticles, creating internanoparticle voids that could be responsible for the increase of the specific surface area and total pore volume of the samples. Furthermore [47], a large specific surface preadsorbs more organic molecules on the surface, which helps to reduce the recombination of photogenerated electrons and holes, improving the efficiency of the photocatalytic degradation. Furthermore, the surface area can be correlated with the number of the active sites. Therefore, the larger S_{BET} of TiO$_2$/activated carbon indicates that this composite could be very promising in the degradation of organic pollutants. [48, 49].

Table 2 shows the specific surface area (S_{BET}) and total pore volume of all samples. It can be seen that the photocatalysts containing activated carbon had a larger S_{BET} and total pore volume than the samples without activated carbon. The specific surface area and total pore volume play an important role in determining the activity of photocatalysts because it is a surface-based phenomenon [50–52].

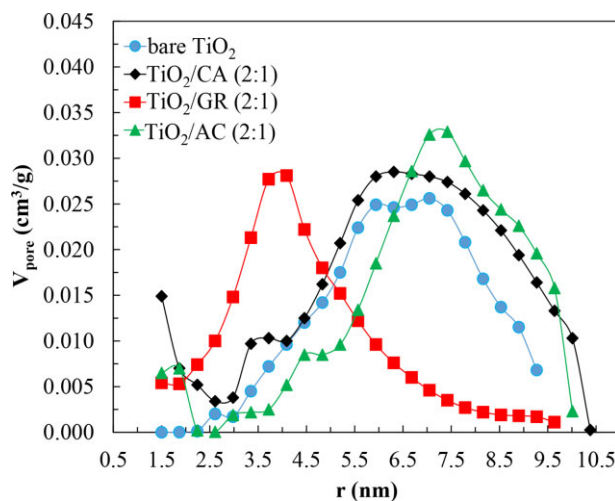**Figure 1** Diffuse reflectance spectra of the composite photocatalysts TiO$_2$/graphite.
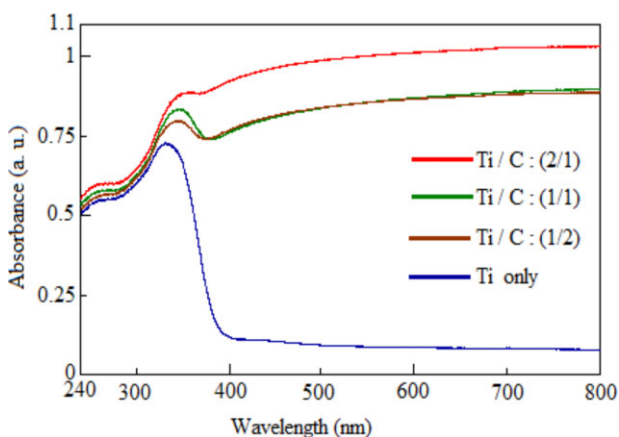
Figure 3 Diffuse reflectance spectra of the composite photocatalysts TiO$_2$/carbon aerogel.

Phys. Status Solidi B 252, No. 11 (2015)

2507
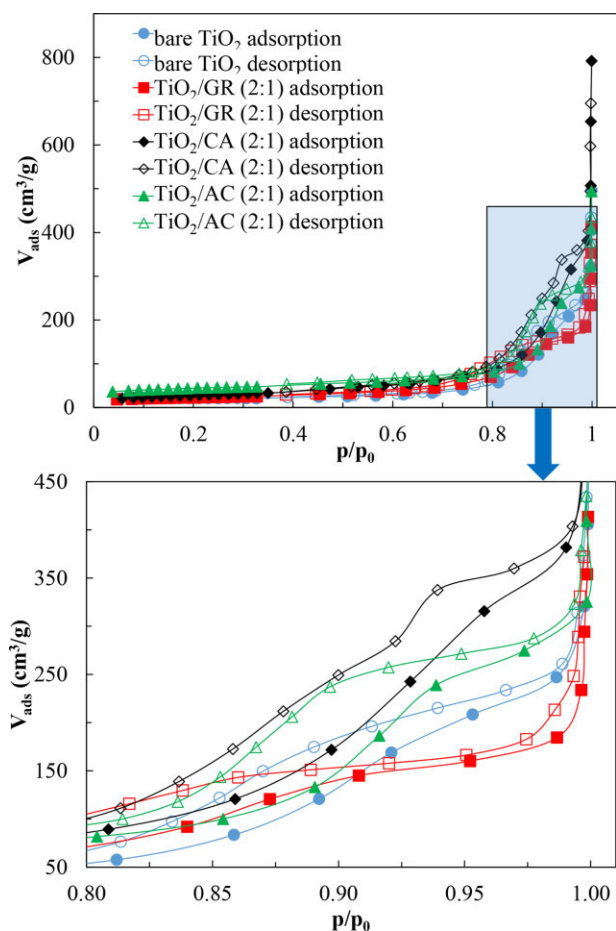
Figure 4 Nitrogen adsorption–desorption isotherms of the samples.

Figure 5 Pore-size distributions of samples.

3.1.3 X-ray diffraction analysis and TEM As it is well known, crystallinity plays a very important role in the photocatalytic activity of titania. Better crystallinity can decrease the number of crystal defects, which is supposed to be the recombination center of the photogenerated electrons and holes. Therefore, better crystallinity can improve the photocatalytic activity of titania [47].

In this study, we used a commercial P25 powder, a reference photocatalyst, for comparing the properties of synthesized samples. Commercial titanium dioxide's crystallite size was determined to be 25 nm and consisted of 80% anatase and 20% rutile with a total specific surface area of $50 \, m^2 \, g^{-1}$.

The XRD patterns of the prepared samples are shown in Fig. 6. Anatase and rutile phases (in commercial TiO_2 powder, not shown here) presented the following diffraction peaks: a major intensity signal associated with the reflection, located at $2\theta = 25.30°$ representing anatase (101) peak and at $2\theta = 27.43°$ that represents the rutile (110) peak, as well as other important anatase signals at $2\theta = 37.79°$, $48.04°$, $53.88°$, $55.06°$. The synthesized nanoparticles dominant crystal phase was anatase (A). The strongest peak was observed for the anatase (101) reflection at $2\theta = 25.3°$. However, some brookite was also detected in some of the samples, as shown by the distinctive B (211) reflection at $2\theta = 30.6°$. In Fig. 6 a graphite-related peak GR (002) at 26.6 (2θ) was also clearly detectable.

Crystallite size and weight percentage of crystalline phases of the samples calculated from the XRD patterns are listed in Table 3. We observed that the size of the crystals in the composites is in the same range and independent of the preparation method. We obtained predominantly the anatase crystalline phase.

The success of the TiO_2 deposition process was also verified by TEM. All the TEM confirmed was what already suggested by the other measurement techniques, that the synthesis process was successful. The most interesting structural build-up was shown by the TiO_2/CA composites. In the TEM micrographs (Fig. 7) the amorphous carbon aerogel can be seen in the background in which the TiO_2 nanocrystals are embedded.

Table 2 The calculated structural parameters from the N_2 adsorption isotherms.

sample name	ratio Ti/C	S_{BET} (m^2/g)	total pore volume (cm^3/g)
TiO_2/GR	(1/1)	113	0.243
TiO_2/GR	(1/2)	143	0.230
TiO_2/GR	(2/1)	52	0.079
TiO_2/AC	(1/1)	338	0.333
TiO_2/AC	(1/2)	300	0.334
TiO_2/AC	(2/1)	214	0.342
TiO_2/CA	(1/1)	143	0.230
TiO_2/CA	(1/2)	154	0.309
TiO_2/CA	(2/1)	206	0.310
TiO_2	(1/0)	95	0.285
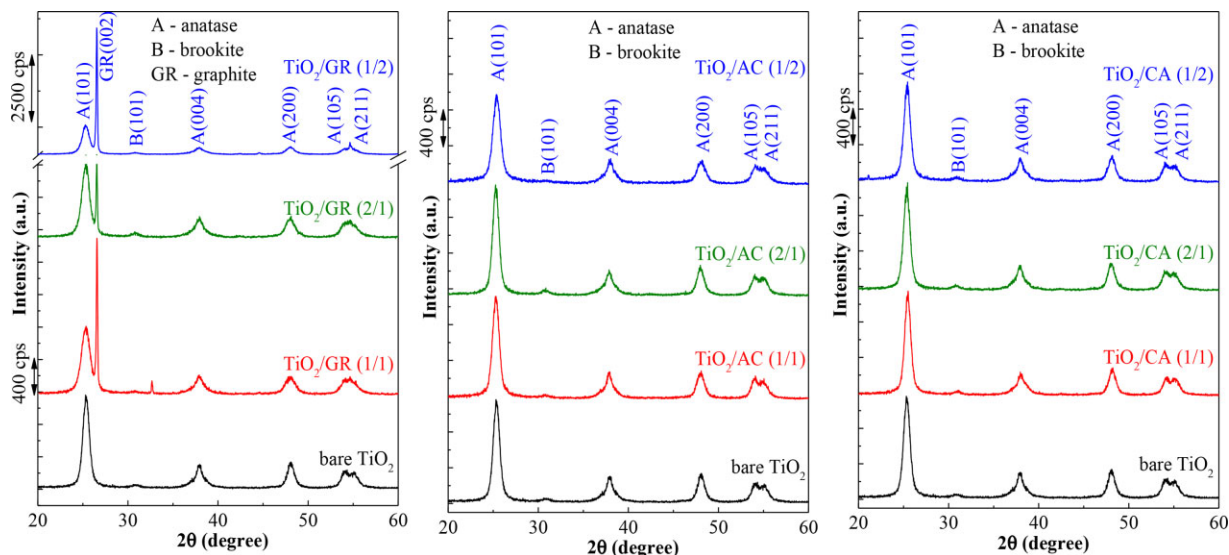
Figure 6 XRD patterns of all the studied samples.

This connection between the materials clearly emphasizes that the CA-containing composites can enrich the pollutant concentration near the semiconductor nanoparticles resulting in an enhanced photocatalytic activity. More precisely, this means that around the TiO_2 nanocrystals a constant and high concentration of pollutant molecules will be found during the degradation process.

3.2 Photocatalytic activity Figure 8 shows the photocatalytic degradation rates of diuron, which are equal to the differences between the total degradation rate under illumination and the adsorption degradation rate in the dark.
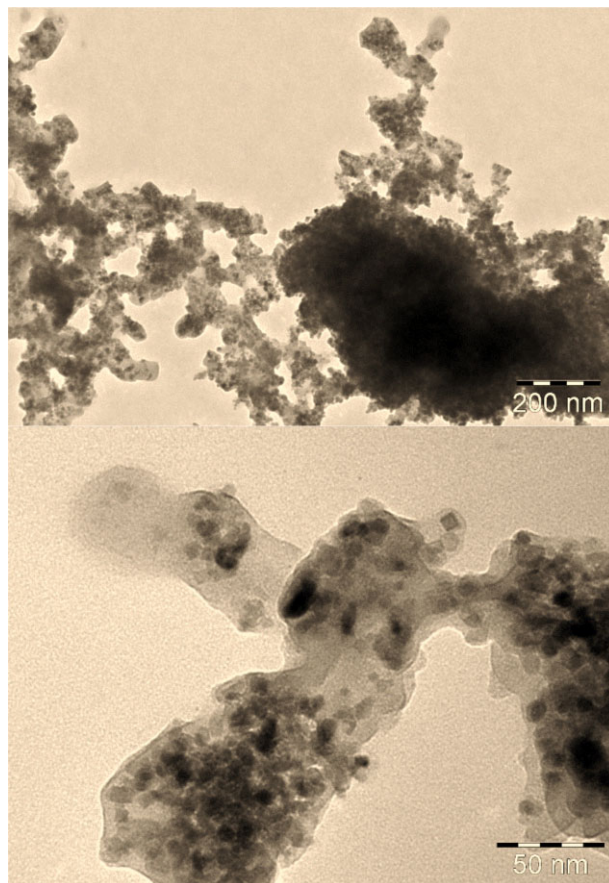
Compared with the photocatalytic degradation, the direct photolysis of the diuron is negligible. It can be seen that unmodified titania, commercial P25 powder, and TiO_2/CA (2/1) exhibit the highest photocatalytic activity, which is attributed to its high anatase crystallinity. However, it does not exceed the activity of the commercial P25 powder. The photocatalytic reactions depend on the induction of the

charge carriers of titania. On the basis of the above characterization results and the photocatalytic degradation data, the activity enhancement mechanism of the modified titania can be suggested. The mechanism is mainly involved
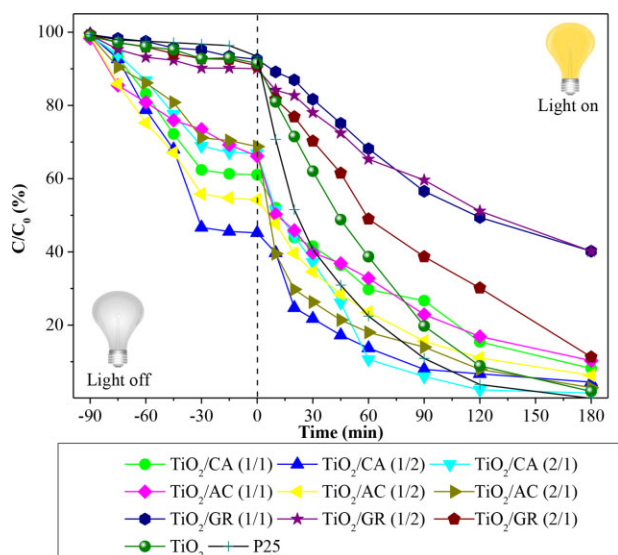

Figure 7 TEM micrographs of sample TiO_2/CA (1:1).

Table 3 The evaluation of the XRD results.

sample name	ratio Ti/C	anatase (wt%)	brookite (wt%)	graphite (wt%)
TiO_2/GR	(1/1)	91.3	0.2	8.5
TiO_2/GR	(1/2)	82.3	1.6	16.1
TiO_2/GR	(2/1)	94.7	1.2	4.1
TiO_2/AC[a]	(1/1)	99.6	0.4	0
TiO_2/AC[a]	(1/2)	99.8	0.2	0
TiO_2/AC[a]	(2/1)	99.2	0.8	0
TiO_2/CA[a]	(1/1)	99.4	0.6	0
TiO_2/CA[a]	(1/2)	99.1	0.9	0
TiO_2/CA[a]	(2/1)	99.2	0.8	0
TiO_2	(1/0)	99.4	0.6	0

[a]Carbon content not evaluated with XRD.

Phys. Status Solidi B 252, No. 11 (2015)

Original

Paper

2509

Figure 8 The photocatalytic degradation of diuron under artificial light.

Figure 9 The photocatalytic degradation of diuron under sunlight.

with the high photoinduced charge separation rate. Besides the high photoinduced charge separation rate, the large surface area is also favorable to enhance photocatalytic activity. The TiO_2/AC (2/1) ($214\,m^2\,g^{-1}$) and the TiO_2/CA (1/2) ($154\,m^2\,g^{-1}$) composites have a larger BET surface area than commercial P25 powder (about $55\,m^2\,g^{-1}$). Therefore, the final photocatalytic performance depends on the combination effects of the photoinduced charge-separation situation and the surface area.

The diuron photodegradation kinetic on TiO_2 (or TiO_2/carbon) under UV irradiation has been associated with the Langmuir–Hinshelwood equation. When the solution is highly diluted, the reaction is essentially an apparent first-order reaction and after integration, the L–H equation can be reduced to the following equation: $\ln(C_0/C) = k_{ap}t$, where k_{ap} is the apparent rate constant of a pseudofirst-order

reaction. By plotting $\ln(C_0/C)$ versus t, the apparent rate constant (k_{ap}) can be determined from the slope of the curve obtained (Table 4).

Table 4 shows that adding carbon has an effect on the disappearance kinetics of diuron. It seems that the presence of other carbon as graphite improves the efficiency of diuron photodegradation, especially with TiO_2/C catalysts (2/1).

Moreover, the photodegradation of diuron was performed under solar irradiation in Abidjan. Because, in a tropical country, like in Ivory Coast there is abundant sunshine and especially in the dry season (December–March). The experiment focused on the catalysts (TiO_2/GR (2/1), TiO_2/AC (2/1), TiO_2/CA (2/1), TiO_2 only) that showed, for each group, the best photocatalytic activity in previous experiments.

The investigation focused on the catalysts (TiO_2/GR (2/1), TiO_2/AC (2/1), TiO_2/CA (2/1), TiO_2) that showed, from each sample group, the best photocatalytic activity in previous experiments. The obtained results are shown in Fig. 9. It is noted that all samples, except for the

Table 4 Apparent first-order rate constant k_{ap}.

materials	under artificial light			under sunlight	
	C/C_0 (%)	$k_{ap} \times 10^2$ (min^{-1})	R^2	$k_{ap} \times 10^2$ (min^{-1})	R^2
TiO_2/GR (1/1)	40.78	0.5	0.98	–	–
TiO_2/GR (1/2)	41.26	0.5	0.99	–	–
TiO_2/GR (2/1)	11.75	1.1	0.98	1.9	0.98
TiO_2/AC (1/1)	10.41	1.2	0.99	–	–
TiO_2/AC (1/2)	6.31	1.3	0.99	–	–
TiO_2/AC (2/1)	3.51	2.3	0.97	2.5	0.99
TiO_2/CA (1/1)	8.77	1.1	0.99	–	–
TiO_2/CA (1/2)	4.84	1.6	0.97	–	–
TiO_2/CA (2/1)	1.39	2.3	0.98	2.6	0.96
bare TiO_2	2.03	2.2	0.99	2.3	0.99
TiO_2 P25	0.05	2.6	0.99	–	–

TiO$_2$/graphite (Ti/C = 2/1), have better photocatalytic activities than the reference photocatalyst (commercial P25 powder). The photocatalytic activities of these materials remain almost identical under artificial and solar irradiation. This clear improvement of the photocatalytic activity, under solar irradiation, may be due to the synergistic effect between the carbon material and TiO$_2$.

Indeed, all catalysts have their absorption region extending from the UV region to the visible, due to the carbon presence (Figs. 1–3). However, excess amount of carbon prevents TiO$_2$ from absorbing UV (samples TiO$_2$/C = 1/2). If there is no UV absorption for TiO$_2$ the sample cannot show any photocatalytic activity. The carbon presence in the nanocomposites also play both the role to prevent e^-/h^+ recombination (by electron transfer from TiO$_2$ to carbon), and provide a large surface area to lead to more hydroxyl group on the surface of TiO$_2$/carbon. Therefore, the addition of an appropriate amount of carbon can greatly improve the photocatalytic activity of TiO$_2$.

The percentages of residual pollutant after 3 h of solar irradiation are respectively 12.52, 18.78, 1.01, and 1.05 when we used the catalysts: TiO$_2$ only, TiO$_2$/GR (2/1), TiO$_2$/AC (2/1), and TiO$_2$/CA (2/1). The lowest performing photocatalyst was the commercial P25 powder because TiO$_2$ alone cannot absorb in the visible region.

4 Conclusions The present study presents a green, cost-effective approach, capable of producing titania/carbon composites. The TiO$_2$ nanoparticles were synthesized by a sol–gel method and the synthesis parameters were examined to approach to the best quality of the product according to the crystallinity, anatase phase content, and the average crystallite size. It is clear that the obtained composites absorb light in the UV region and can be excited in the visible region. All the obtained photocatalysts generally showed a good activity in the photocatalytic degradation of diuron. The samples of TiO$_2$/activated carbon (Ti/C = 2/1), TiO$_2$/carbon aerogel (Ti/C = 2/1) were promising under sunlight irradiation driven diuron degradation among all samples, which can be attributed to the anatase phase, high specific surface area, large pore volume, and their capacities to absorb in the visible-light region.

References

[1] J. Carreno, A. Rivas, A. Granada, and F. Olea-Serrano, Environ. Res. **103**, 55–61 (2007).

[2] A. J. Nozik, Chem. Phys. Lett. **457**, 3 (2008).

[3] K. F. Mak, C. Lee, J. Hone, J. Shan, and T. F. Heinz, Phys. Rev. Lett. **105**, 136805 (2010).

[4] U. G. Akpan and B. H. Hameed, J. Hazard. Mater. **170**, 520 (2009).

[5] A. Matsuda, S. Sreekantan, and W. Krengvirat, J. Asian Ceram. Soc. **1**, 203 (2013).

[6] J. Barber and P. D. Tran, J. R. Soc. Interfaces **10**, 20120984 (2013).

[7] K. Vajda, Z. Kása, A. Dombi, Z. Németh, G. Kovács, V. Danciu, T. Radu, C. Ghica, L. Baia, K. Hernádi, and Z. Pap, Nanoscale **7**, 5776 (2015).

[8] M. M. Mohamed and M. S. Al-Sharif, Appl. Catal. B, Environ. **142–143**, 432 (2013).

[9] T. Tachikawa, M. Fujitsuka, and T. Majima, J. Phys. Chem. C **111**, 5259 (2007).

[10] Y. Luan, L. Jing, J. Wu, M. Xie, and Y. Feng, Appl. Catal. B, Environ. **147**, 29 (2014).

[11] S. M. Miranda, G. E. Romanos, V. Likodimos, R. R. N. Marques, and E. P. Favvas, Appl. Catal. B, Environ. **147**, 65 (2014).

[12] A. Fujishima, T. N. Rao, and D. A. Tryk, J. Photochem. Photobiol. C **1**, 1 (2000).

[13] K. Bubacz, E. Kusiak-Nejman, B. Tryba, and A. W. Morawski, J. Photochem. Photobiol. A **261**, 7 (2013).

[14] M. L. Chen, F. J. Zhang, and W. C. Oh, New Carbon Mater. **24**, 159 (2009).

[15] C. Wang, R. L. Thompson, J. Baltrus, and C. Matranga, J. Phys. Chem. Lett. **1**, 48 (2010).

[16] J. Yu, G. Dai, Q. Xiang, and M. Jaroniec, J. Mater. Chem. **21**, 1049 (2011).

[17] Q. Xiang, J. Yu, W. Wang, and M. Jaroniec, Chem. Commun. **47**, 6906 (2011).

[18] É. Karácsonyi, L. Baia, A. Dombi, V. Danciu, K. Mogyorósi, L. C. Pop, G. Kovács, V. Coşoveanu, A. Vulpoi, S. Simon, and Zs. Pap, Catal. Today **208**, 19 (2013).

[19] P. Wang, D. J. Wang, H. Y. Li, T. F. Xie, H. Z. Wang, and Z. L. Du, J. Colloid. Interf. Sci. **314**, 337 (2007).

[20] X. B. Chen and S. S. Mao, J. Nanosci. Nanotechnol. **6**, 906 (2006).

[21] C. Lao, L. Y. Chuai, L. Su, X. Liu, L. Huang, H. Cheng, and D. Zou, Sol. Energy Mater. Sol. Cells **85**, 457 (2005).

[22] G. S. Li, L. P. Li, J. Boerio-Goates, and B. F. Woodfield, J. Am. Chem. Soc. **127**, 8659 (2005).

[23] M. Niederberger, M. H. Bartl, and G. D. Stucky, Chem. Mater. **14**, 4364 (2002).

[24] N. Serpone, D. Lawless, and R. Khairutdinov, J. Phys. Chem. **99**, 16646 (1995).

[25] Z. Abbas, J. P. Holmberg, A. K. Hellstrom, M. Hagstrom, J. Bergenholtz, M. Hassellov, and E. Ahlberg, Colloids Surf. A **384**, 254 (2011).

[26] Y. X. Chuan, M. Hirano, and M. Inagaki, Appl. Catal. B, Environ. **51**, 255 (2004).

[27] Y. Li, M. Ma, S. Sun, X. Wang, W. Yan, and Y. Ouyang, Catal. Commun. **9**, 1583 (2008).

[28] D. Panayotov, P. Kondratyuk, and J. T. Yates, Langmuir **20**, 3674 (2004).

[29] B. Wu, R. Yuan, and X. Fu, J. Solid State Chem. **182**, 560 (2009).

[30] B. Gao, P. S. Yap, T. M. Lim, and T. T. Lim, Chem. Eng. J. **171**, 1098 (2011).

[31] T. T. Lim, P. S. Yap, M. Srinivasan, and A. G. Fane, Crit. Rev. Environ. Sci. Technol. **41**, 1173 (2011).

[32] J. Matos, J. Laine, J. M. Herrmann, D. Uzcategui, and J. L. Brito, Appl. Catal. B, Environ. **70**, 461 (2007).

[33] B. Tryba, A. W. Morawski, and M. Inagaki, Appl. Catal. B, Environ. **41**, 427 (2003).

[34] T. Cordero, J. M. Chovelon, C. Duchamp, C. Ferronato, and J. Matos, Appl. Catal. B, Environ. **73**, 227 (2007).

Phys. Status Solidi B 252, No. 11 (2015)

Original

Paper

2511

[35] P. Atheba, D. Robert, A. Trokourey, D. Bamba, and J. V. Weber, Water Sci. Technol. **60**, 2187 (2009).

[36] S. Giacomazzi and N. Cochet, Chemosphere **56**, 1021 (2004).

[37] S. Salvestrini, P. Di Cerbo, and S. Capasso, Chemosphere **48**, 69 (2002).

[38] M. Hincapié, M. I. Maldonado, I. Oller, W. Gernjak, J. A. S. Perez, M. M. Ballesteros, and S. Malato, Catal. Today **101**, 203 (2005).

[39] D. Bamba, B. Dongui, A. Trokourey, G. E. Zoro, G. P. Athéba, D. Robert, and J. V. Wéber, J. Soc. Ouest-Afr. Chim. **28**, 41 (2009).

[40] L. C. Cotet, A. Roig, I. C. Popescu, V. Cosoveanu, E. Molins, and V. Danciu, Rev. Roumaine Chim. **52**, 1077 (2007).

[41] H. Zhang and J. F. Banfield, J. Phys. Chem. B **104**, 3481 (2000).

[42] D. Bamba, P. Atheba, D. Robert, A. Trokourey, and B. Dongui, Environ. Chem. Lett. **6**, 167 (2008).

[43] Y. Liu, Y. Li, Y. T. Wang, L. Xie, J. Zheng, and X. G. Li, J. Hazard. Mater. **150**, 153 (2008).

[44] T. Sreethawong, Y. Yamada, T. Kobayashi, and S. Yoshikawa, J. Mol. Catal. A **241**, 23 (2005).

[45] J. C. Yu, L. Zhang, and J. Yu, Chem. Mater. **14**, 4647 (2002).

[46] J. W. Shi, X. Yan, H. J Cui, X. Zong, M. L. Fu, S. Chen, and L. Wang, J. Mol. Catal. A, Chem. **356**, 53 (2012).

[47] J. W. Shi, J. T. Zheng, and P. Wu, J. Hazard. Mater. **161**, 416 (2009).

[48] Y. Chen and D. D. Dionysiou, J. Mol. Catal. A, Chem. **244**, 73 (2006).

[49] M. M. Ba-Abbad, A. A. H. Kadhum, A. B. R. Mohamad, M. S. Takriff, and K. Sopian, Int. J. Electrochem. Sci. **7**, 4871 2012.

[50] S. C. Jung, S. J. Kim, N. Imaishi, and Y. I. Cho, Appl. Catal. B, Environ. **55**, 253 (2005).

[51] K. Nakata and A. Fujishima, J. Photochem. Photobiol. C **13**, 169 (2012).

[52] M. A. Henderson, Surf. Sci. Rep. **66**, 185 (2011).